analytical chemistry

Article

Cite This: Anal. Chem. 2018, 90, 6477−6485

pubs.acs.org/ac

Analysis of Ag(I) Biocide in Water Samples Using Anodic Stripping Voltammetry with a Boron-Doped Diamond Disk Electrode

Vanessa Y. Maldonado,[†,⊥] Patricio J. Espinoza-Montero,[‡,§] Cory A. Rusinek,[∥] and Greg M. Swain*[,⊥]

[†]Facultad de Ingeniería Química y Agroindustria, Escuela Politécnica Nacional, Ladrón de Guevara E11-253, P.O. Box 17-01-2759, Quito 170525, Ecuador

[‡]Escuela de Ciencias Químicas, Pontificia Universidad Católica del Ecuador, Avenida 12 de octubre y Roca, P.O. Box 17-01-2184, Quito, Ecuador

[§]Departamento de Ingeniería Civil y Ambiental, Escuela Politécnica Nacional, Ladrón de Guevara E11-253, P.O. Box 17-01-2759, Quito, Ecuador

[∥]Fraunhofer Center for Coatings and Diamond Technologies, Michigan State University, East Lansing, Michigan 48824 United States

[⊥]Department of Chemistry, Michigan State University, East Lansing, Michigan 48824, United States

Supporting Information

ABSTRACT: The electroanalytical performance of a new commercial boron-doped diamond disk and a traditional nanocrystalline thin-film electrode were compared for the anodic stripping voltammetric determination of Ag(I). The diamond disk electrode is more flexible than the planar film as the former is compatible with most electrochemical cell designs including those incorporating magnetic stirring. Additionally, mechanical polishing and surface cleaning are simpler to execute. Differential pulse anodic stripping voltammetry (DPASV) was used to detect Ag(I) in standard solutions after optimization of the deposition potential, deposition time and scan rate. The optimized conditions were used to determine the concentration of Ag(I) in a NASA simulated potable water sample and a NIST standard reference solution. The electrochemical results were validated by ICP-OES measurements of the same solutions. The detection figures of merit for the disk electrode were as good or superior to those for the thin-film electrode. Detection limits were ≤5 μg L^{-1} (S/N = 3) for a 120 s deposition period, and response variabilities were <5% RSD. The polished disk electrode presented a more limited linear dynamic range presumably because of the reduced surface area available for metal phase formation. The concentrations of Ag(I) in the two water samples, as determined by DPASV, were in good agreement with the concentrations determined by ICP-OES.

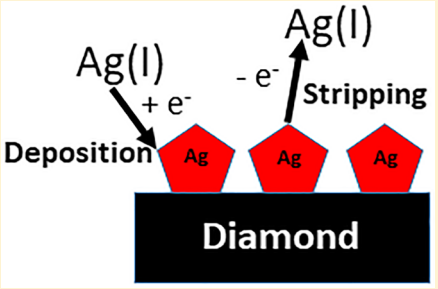

Monitoring toxic metal ion concentrations in soil and water supplies is essential for human health and safety. This can be accomplished electrochemically[1] using various sensing platforms, as our group has shown over the years with boron-doped diamond.[2−6] Silver ion is one metal species of growing importance though. Ionic silver (Ag(I)) is an effective biocide so it is used in present-day consumer items including textiles, personal care products, paints, laundry additives, wound dressings, medicines, medical devices, and water purification systems.[7−9] As a consequence, an estimated 65 tons of silver are released annually into the environment.[9] According to the United States Agency for Toxic Substances and Disease Registry (ATSDR), silver ion levels in surface waters are generally in the range of 0.2−2.0 μg L^{-1}, 200−300 μg L^{-1} in soils, and up to 80 μg L^{-1} in drinking water.[10] The silver used in these applications exists either as Ag(I) or as nanoparticles or colloids of silver metal; the toxicity of which depend on their size.[11,12] Ag(I) can be released into the environment by direct leaching from these sources or via oxidation of the colloidal particles. Concentrations of Ag(I) in water greater than 0.17 μg L^{-1} are toxic to fish and microorganisms.[13] The metal ion is also a known toxicant that causes cytological and adverse physiological effects.[14] As such, the U.S. Environmental Protection Agency (EPA) considers Ag(I) as a secondary contaminant and has established 100 μg L^{-1} as the maximum contaminant level (sMCL) allowed in drinking water.[15] The increasing use of this biocide in commercial products is going to produce a future need for fast, inexpensive and reliable analysis of Ag(I) analysis in soil and water samples.

While the emergence of Ag(I) as a potential pollutant is driving current work, our original interest in this metal ion stems from work performed to develop an electrochemical method for its detection using a boron-doped electrode that could be used on-board the International Space Station (ISS). At the time, there was a significant need for Ag(I) analysis because of its use as a biocide on ISS in the water treatment system. Two potable water disinfection systems continue to be

Received: November 30, 2017
Accepted: May 14, 2018
Published: May 14, 2018

DOI: 10.1021/acs.analchem.7b04983
Anal. Chem. 2018, 90, 6477−6485

used on ISS.[16,17] The American segment uses iodine salts with little mineralization while the Russian segment uses silver salts and heavy mineralization (Mg(II) and Ca(II)). The treated potable water originates from two sources: ground-prepared water transported to ISS and water generated on-board from fuel cell operation. Additionally, there are units to collect and process humidity condensate recovered directly from the cabin air. Ag(I) biocide minerals are added to the potable water using a conditioning bed prior to storage. The Ag(I) concentration is maintained in the 300−500 $\mu g\ L^{-1}$ range for maximum effectiveness.[16−19] Potable water is used on-board for drinking, food rehydration and hygiene.[16,17] In the past, analysis of potable water was performed on earth using archived water samples periodically transported back from the ISS. This analytical protocol (multiple month lag times) afforded no possibility of responding quickly to a contamination outbreak. More recently, a colorimetric solid-phase extraction (CSPE) method has been introduced and tested on-board ISS for monitoring total Ag.[18−22] CPSE is a sorption-spectrophotometric technique that combines colorimetric reagents, solid-phase extraction and diffuse reflectance spectroscopy to quantitate trace levels of target analytes in water samples.[18−22] Therefore, there is no longer a need for a space-based assay for Ag(I).

Anodic stripping voltammetry (ASV) is an analytical method that has been widely employed for the analysis of trace metal ions in water due to the method's high sensitivity, simplicity and portability.[1,12] Mercury has historically been the electrode of choice for metal ion analysis by ASV.[23,24] Despite its excellent performance in this analytical measurement, the metal is toxic and volatile. Additionally, mercury is ineffective for the detection of Ag(I) as oxidation or stripping of the analyte occurs at potentials positive of where mercury undergoes oxidation. Several electrodes have been investigated as more environmentally friendly alternates to mercury for general metal ion analysis including unmodified and chemically modified Au,[25] Bi,[26] carbon nanofibers,[27] carbon nanotubes[28] and modified glassy carbon.[29,30] In addition, the detection of Ag(I) in solution using ASV has been reported for different chemically modified electrodes. For instance, Dong and Wang used a Nafion/crown ether film electrode and achieved a detection limit of 0.3 ng L^{-1} after 30 min of deposition.[31] Zeng et al. used DL-dithiothreitol monolayer-modified gold electrodes and obtained linearity in the range of 64 to 257 $\mu g\ L^{-1}$.[25] Mohadesi and Taher used a carbon paste electrode modified with 3-amino-2-mercapto quinazolin-4(3*H*)-one and obtained a linear range from 0.9 to 300 $\mu g\ L^{-1}$.[32]

Another alternative electrode for ASV that our group[2−6] and others[33−39] have been investigating in recent years is boron-doped diamond (BDD). BDD performs well in electroanalytical measurements, often providing superior detection figures of merit as compared with conventional carbon electrodes.[2,40−44] BDD is characterized by a wide working potential window, low background current and noise, good sensitivity, chemical inertness, excellent stability at positive potentials and high currents, and weak molecular adsorption.[2,40−46] The properties that make it attractive for ASV are (i) the wide cathodic and anodic potential limits, (ii) sluggish electron-transfer kinetics for the reduction of dissolved oxygen (an interference in ASV), and (iii) relatively rapid electron-transfer kinetics for metal deposition and stripping reactions.[3−6] So far, there has been a limited amount published on the use of BDD for Ag(I) analysis by ASV.[3] One other nontraditional electrode that has been used for Ag(I) analysis is porous GaN.[47] For this electrode, a linear dynamic range from 1 to 100 $\mu g\ L^{-1}$ and a limit of detection of 0.5 $\mu g\ L^{-1}$ were reported.

In the present work, the analysis of Ag(I) in different water samples was performed by differential pulse ASV (DPASV) to demonstrate the performance of the commercial diamond disk electrode. Comparison measurements were performed using a traditional polycrystalline BDD thin-film electrode deposited in-house. The diamond disk is an easy-to-use electrode that consists of a polished, free-standing electrode sealed in a polyether ether ketone (PEEK) plastic body (6 cm length × 6 mm O.D). A metal rod mounted in the plastic body is used for electrical connection to the backside of the electrode. The diamond disk electrode allows more flexibility in measurements than does the traditional BDD thin-film electrode deposited on a conducting substrate in terms of compatibility with wide range of electrochemical cell designs, enabling the use of magnetic stirrers, and enabling the use of mechanical polishing to clean and refresh the surface. It is the earth-bound need that defines the merit of this work.

EXPERIMENTAL SECTION

Boron-Doped Nanocrystalline Diamond Thin-Film Electrode. The boron-doped nanocrystalline diamond planar film was deposited on a boron-doped p-Si(100) ($\sim 10^{-3}\ \Omega$·cm, Virginia Semiconductor, Inc., Fredricksburg, VA) substrate, using a commercial microwave-assisted CVD system (1.5 kW Seki Technotron). The film was deposited using a 1% CH_4/H_2 (v/v) source gas ratio with 10 ppm of boron added for doping in the form of 0.1% B_2H_2 diluted in H_2. The deposition pressure was 35 Torr and the microwave power was 800 W. The deposition time was 5 h. The temperature was estimated to be 825 °C using a disappearing-filament optical pyrometer. The gas flow rates were 2.00 sccm CH_4, 2.00 sccm B_2H_6 diluted in H_2 (0.1%), and 196 sccm H_2. The film thickness using these growth conditions was 3−4 μm based on the mass increase of the substrate after deposition, assuming a density of 3.51 g cm^{-3}, and measurements by digital microscopy. The nominal crystallite size in the film was ≤100 nm.

Boron-Doped Diamond Disk Electrode. The commercial disk electrode was prepared by a proprietary process at the MSU-Fraunhofer Center for Coatings and Diamond Technologies. A multistep construction process was used that involved preparation of a free-standing conducting diamond plate, polishing the polycrystalline diamond plate, laser cutting a circular disk of diamond, and mounting it inside of a PEEK holder with adhesive and sealant epoxy. A Cu wire was inserted in the backside of the PEEK that served as the current collector to the diamond electrode.

Electrochemistry. All electrochemical measurements were performed using a CHI potentiostat (Model 832A, Austin, Texas). The electrochemical cell was placed inside a Faraday cage for shielding. A single-compartment (ca. 10 mL volume) three-electrode glass cell was used that consisted of a BDD working electrode, a graphite rod counter electrode and a commercial Ag/AgCl (3 mol L^{-1} KCl) reference electrode (E = −0.045 V vs SCE (standard calomel electrode)). The diamond film working electrode was pressed against a Viton O-ring and clamped to the bottom of a glass cell. Ohmic contact was made by pressing a Cu plate against the backside of the scratched and cleaned conducting Si substrate. A layer of graphite from a pencil was applied to the backside of the substrate to produce good ohmic contact with the Cu metal. The geometric area of

DOI: 10.1021/acs.analchem.7b04983
Anal. Chem. 2018, 90, 6477−6485

the thin-film electrode was 0.2 cm^2. The BDD disk electrode was used in the same cell and had a geometric area of 0.031 cm^2. It was prepared for use by mechanical polishing for 2 min using successively smaller diameter alumina powder (0.3 and 0.05 μm, Buehler Limited, IL) slurried in ultrapure water. The polishing was performed on separate and clean felt pads. After each polishing step, the electrode was rinsed copiously with ultrapure water and ultrasonically cleaned (suspended in the vibrating liquid) in the same medium for 10 min to remove polishing debris from the surface. As a final step, the BDD electrode surface was contacted with ultrapure (distilled and purified over activated carbon) isopropanol in the electrochemical cell for 20 min. The cell was then rinsed with ultrapure water and filled with the appropriate analyte solution prior to a measurement. Pretreatment is generally not needed to activate BDD electrodes. It was used in this work to test the integrity of the diamond/epoxy/PEEK contact over time.

All measurements were performed at room temperature (ca. 23−25 °C). All solutions were purged with pure N_2 for at least 10 min and then blanketed with the gas during a measurement. The supporting electrolyte was 0.1 mol L^{-1} sodium acetate buffer, pH 4.6. The ASV measurements used a selected deposition time, followed by a 20 s "quiet" time before initiation of the anodic sweep. The differential pulse voltammetric settings for the anodic sweep were: pulse height = 50 mV, step height = 4 mV, pulse width = 50 ms, and cycle period = 100 ms. A constant potential of 600 mV for 180 s was applied after completion of the anodic sweep to fully oxidize all metal deposits prior to the next measurement

ICP-OES Analysis. Inductively coupled plasma optical emission spectroscopy (ICP-OES) was also used to quantify Ag(I) in the different water samples. The silver ion concentrations were determined quantitatively using response curves generated from external standards. Each standard was prepared from a 1000 mg L^{-1} commercial Ag(I) stock solution (Fischer CAS No.7761−88−8) and diluted appropriately using 2% nitric acid. Standard solutions from 5 to 500 μg L^{-1} were prepared. The elemental analysis was performed using a Varian 710-ES ICP-OES with a SPS 3 autosampler. The standard solutions were analyzed first in order of increasing concentration. This was followed by analysis of the unknown. The rinse solution was 2% nitric acid. The peak intensities of selected emission lines were used to construct calibration curves.

NIST Reference Solution. One water sample analyzed was a reference material (#1640, henceforth referred to as SRM 1640) that was procured for testing (2005) from the National Institute of Standards and Technology (NIST). The aqueous sample contained certified amounts of Ag(I), in addition to at least 24 other dissolved elements. The certified value of Ag(I) was 7.62 ± 0.25 μg L^{-1}.

NASA Water Samples. Simulated ISS potable water samples were provided (Feb. 2005) by Wyle Laboratories (Houston, Texas). The potable samples contained minerals Ca(II) and Mg(II) as formate salts and Ag(I), analogous to groundwater prepared for transport to ISS. The samples were stored in a dark plastic bottle in the refrigerator when not in use. A second sample was also analyzed as a control. This was an Ersatz iodinated water sample that contained 4.38 mg L^{-1} iodine the as a biocide, with no Ag(I) added. This water sample was prepared by the Water and Food Laboratory at the NASA Johnson Space Center (2005).

Chemicals. All solutions were prepared using deionized water produced by a Barnstead E-Pure system (~18 MΩ·cm, Millipore, U.S.A.). Silver sulfate (CAS No. 10294−26−5, ≥ 99.9%), and potassium ferrocyanide(II) hydrate (CAS No. 14459−95−1, ≥99.99%) and potassium chloride (CAS No. 7447−40−7, ≥99%) were all reagent-grade quality used without additional purification. The 0.1 mol L^{-1} acetate buffer (pH 4.6) was prepared by mixing appropriate amounts of sodium acetate (CAS No. 127−09−3, ≥99.9%) and acetic acid (CAS No. 64−19−7, ≥99.9%). All solutions were prepared fresh daily and purged with N_2 (99.99%) for 10 min prior to any electrochemical measurement. All glassware was cleaned using the following procedure: washing in an alconox/ultrapure water solution, soaking in 1 mol L^{-1} hydrochloric acid and 1 mol L^{-1} nitric acid for at least 10 min each and a final rinsing with ultrapure water. The cleaned glassware was then dried in an oven at ~55 °C.

RESULTS AND DISCUSSION

Figure 1 shows the design of the BDD disk electrode. Unlike the traditional planar film, the disk electrode offers some

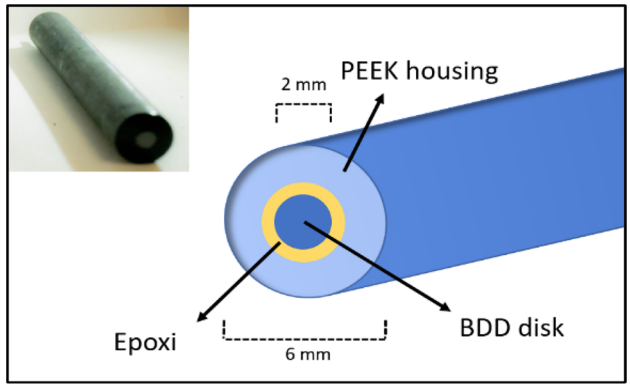

Figure 1. Schematic design of the boron-doped diamond disk electrode. The electrode consists of a polished diamond disk (nm roughness) that is sealed in PEEK housing. The inset shows a photograph of the sealed electrode.

advantages for analytical measurements. One of these is its simplicity. The disk electrode can be used in all types of electrochemical cells and does not require an O-ring and clamp for mounting, as does the thin-film electrode. In addition, the disk electrode can be polished to clean and refresh the surface prior to a measurement. The polishing does not remove "diamond" carbon from the surface but does other material, such as residual metal deposits. One focal point in these studies was assessment of the quality of the seal between the diamond disk and the PEEK holder. Both the planar film and the disk electrode were characterized by cyclic voltammetry using $Fe(CN)_6^{3-/4-}$ as a redox probe molecule. These results are described in the Supporting Information.

Figure 2 shows an SEM micrograph (secondary electron image) of the polished diamond disk electrode after acid cleaning. The film is relatively smooth after the polishing but the large base crystallites and the connecting grain boundaries are still visible. The primary grains or crystallites are 10s of micrometers in lateral dimension.

Figure 3 presents differential pulse voltammetric background i−E curves for the planar film and disk electrodes at potentials between 0 and 0.6 V. This is the potential region where Ag

DOI: 10.1021/acs.analchem.7b04983
Anal. Chem. 2018, 90, 6477−6485

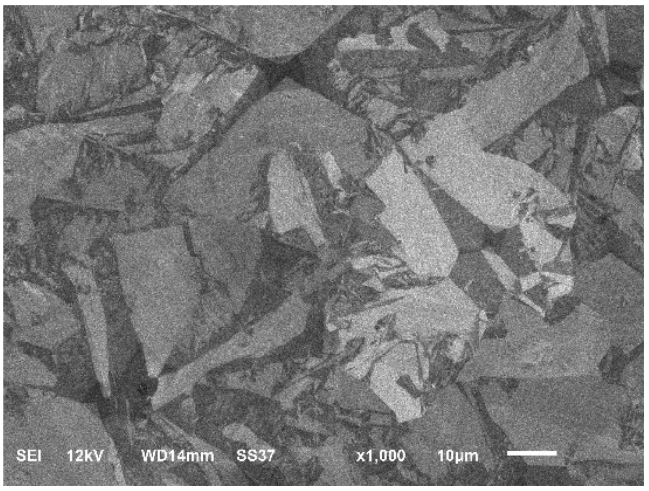

Figure 2. SEM micrograph of the polished polycrystalline diamond disk electrode after acid cleaning.

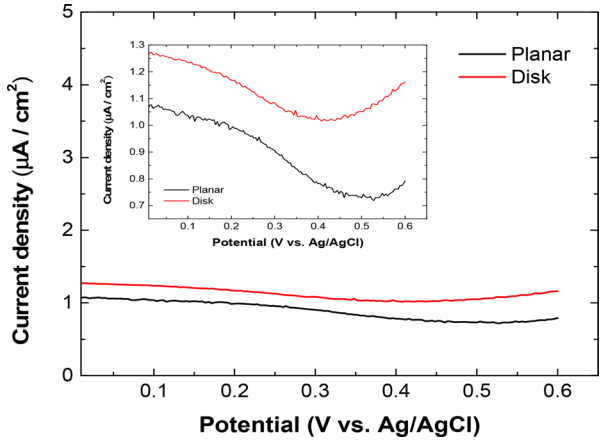

Figure 3. Differential pulse voltammetric background i–E curves for the BDD planar film and disk electrodes in 0.1 mol L^{-1} acetate buffer (pH 4.6) at potentials from 0 to 0.6 V. The curves were recorded using a pulse amplitude of 0.05 V; a potential step of 0.004 V; a pulse width of 50 ms; and a pulse period of 100 ms.

stripping occurs. In comparison to other electrodes, Ag(I) can be detected by ASV with BDD due to its wide anodic potential window.[2,3,40−44] The currents have been normalized to the geometric area of each electrode in contact with the electrolyte solution. The background current for BDD in this potential region is almost exclusively capacitive. The background current density at both electrodes is below 1.3 μA cm^{-2}, with the magnitude for this particular planar electrode being slightly lower than that for the disk electrode. However, when comparing the background current for multiple electrodes, no significant difference was found between the two electrodes. Importantly, the background current density for both diamond electrodes is about 10× lower than the current density for glassy carbon of equivalent geometric area (data not shown). The lower background current for the BDD electrodes is attributed to a lower density of electronic states due to the semimetal electronic properties and the absence of pseudocapacitive current associated with electroactive and or ionizable surface carbon−oxygen functionalities over this potential range. These are inherent characteristics of the sp^3 nature of the BDD electrodes.[2,40−46] Variations in the boron doping level will affect the background current with increasing doping level producing increasing background current.

Effect of Deposition Parameters. In metal phase formation and growth, nuclei of the metal phase must reach a critical size before they become stable on the surface and can serve as sites for growth.[48] The formation of stable metal nuclei can be achieved by (i) applying a negative overpotential with respect to the formal potential, $E^{\circ\prime}$, for the metal/metal ion couple and (ii) having a deposition time long enough at an overpotential to allow the nuclei to reach a critical size.

When using diamond or any other solid electrode for ASV, one has to optimize the metal phase formation over the surface. Ideally, a metal phase consisting of nominally small particles with low size variance, deposited uniformly across the surface is sought. Irregular deposit sizes lead to broadened stripping peaks. The reason for this is that it takes longer during a scan for a large deposit to oxidize as compared to a smaller one. A series of experiments was performed to optimize the deposition potential, deposition time and scan rate in terms of the stripping peak current for Ag(I) and peak width. These optimization experiments were performed using the planar film electrode. Figure 4 shows the influence of the deposition

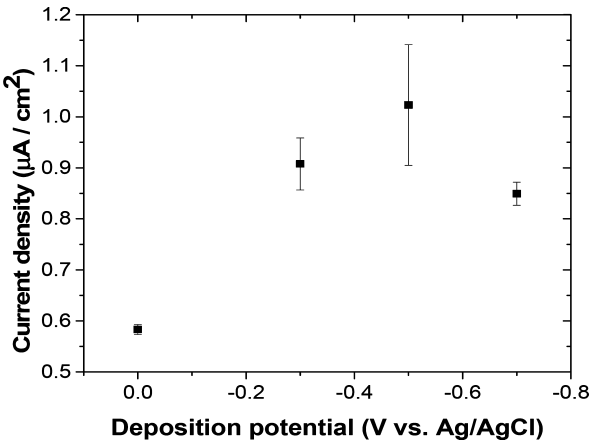

Figure 4. Influence of the deposition potential on the stripping peak current for 50 μg L^{-1} of Ag(I) in 0.1 mol L^{-1} acetate buffer (pH 4.6). The curves were recorded by differential pulse voltammetry using a pulse amplitude of 0.05 V; a potential step of 0.004 V; a pulse width of 50 ms; and a pulse period of 100 ms. Working electrode: BDD planar film. Values are presented as mean ± std. dev. (n = 3 measurements).

potential on the stripping peak current density at potentials from 0 to −0.7 V. As can be seen, the stripping peak current increased with the deposition potential up to −0.5 V. There was no statistical difference in the current magnitude at −0.3 and −0.5 V, but the background current and noise were significantly lower at −0.3 V. For potentials more negative of −0.5 V, a decrease in the peak current was observed. Making the deposition potential more negative increases the driving force or overpotential for metal phase formation. However, at the most negative potentials, other side reactions start to contribute to the current flow including trace oxygen reduction and reduction of water. These competing reactions reduce the amount of metal deposited. Deposition at −0.3 V was selected for the subsequent ASV measurements because it afforded the largest peak amplitude, most narrow peaks, and the lowest noise.

It can be seen in Figure 5 that the peak current increased proportionally with deposition time at −0.3 V between 30 and

DOI: 10.1021/acs.analchem.7b04983
Anal. Chem. 2018, 90, 6477−6485

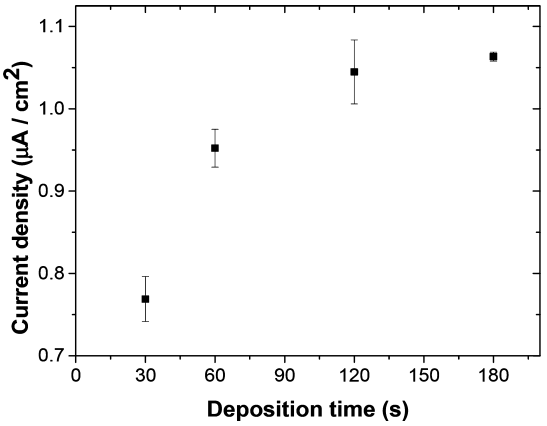

Figure 5. Influence of the deposition time on the stripping peak current for 50 μg L^{-1} Ag(I) in 0.1 mol L^{-1} acetate buffer (pH 4.6). The curves were recorded by differential pulse voltammetry using a pulse amplitude of 0.05 V; a potential step of 0.004 V; a pulse width of 50 ms; and a pulse period of 100 ms. Working electrode: BDD planar film. Values are presented as mean ± std. dev. (n = 3 measurements).

120 s. After 120 s, the peak current leveled off. The stripping charge (not shown) also increased proportionally with the deposition time. Above 120 s, the peaks became broader without increasing much in current magnitude. This is due, in part, to peak broadening that results from saturation of the available surface sites on the BDD electrode for the Ag deposition. This leads to significant metal on metal deposition and likely a variable deposit size across the surface.[2−4,49] Based on these results and considering that even if the peak currents were to increase, long deposition times are undesirable for a real analysis. Therefore, a deposition time of 120 s was selected for use in the subsequent ASV measurements.

Figure 6 shows how the Ag(I) stripping peak current density changes with the effective scan rate. The optimized parameters for deposition potential and time, as reported above, were used (−0.3 V and 120s). The effective scan rate was adjusted by changing the potential step height (V) in the differential pulse

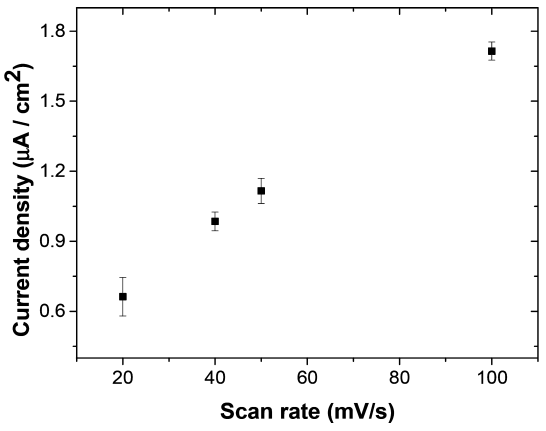

Figure 6. Influence of the scan rate on the stripping peak current for 50 μg L^{-1} Ag(I) in 0.1 mol L^{-1} acetate buffer (pH 4.6). The deposition potential was −0.3 V and the deposition time was 120 s. The curves were recorded by differential pulse voltammetry using a pulse amplitude of 0.05 V; a varying potential step of 0.002 to 0.010 V; a pulse width of 50 ms; and a pulse period of 100 ms. Working electrode: BDD planar film. Values are presented as mean ± std. dev. (n = 3 measurements).

method from 2 to 10 mV (20 to 100 mV s^{-1}), while maintaining a pulse period of 100 ms. A linear relationship between the Ag stripping peak current and the scan rate (i.e., step height) was seen. Increased scan rate produced increased peak current. However, additional experiments, performed with different concentrations of Ag(I), showed that scan rates in excess of 40 mVs^{-1} produced poor stripping peak current reproducibility. For this reason, 40 mVs^{-1} was selected as the optimum effective scan rate for the measurements.

DPASV Analysis of Standard Solutions. Standard solutions of Ag(I) were used to generate response curves for the BDD planar film and disk electrodes. The experimental conditions used were the optimum ones described above. Figure 7 shows representative DPASV i−E curves as a function

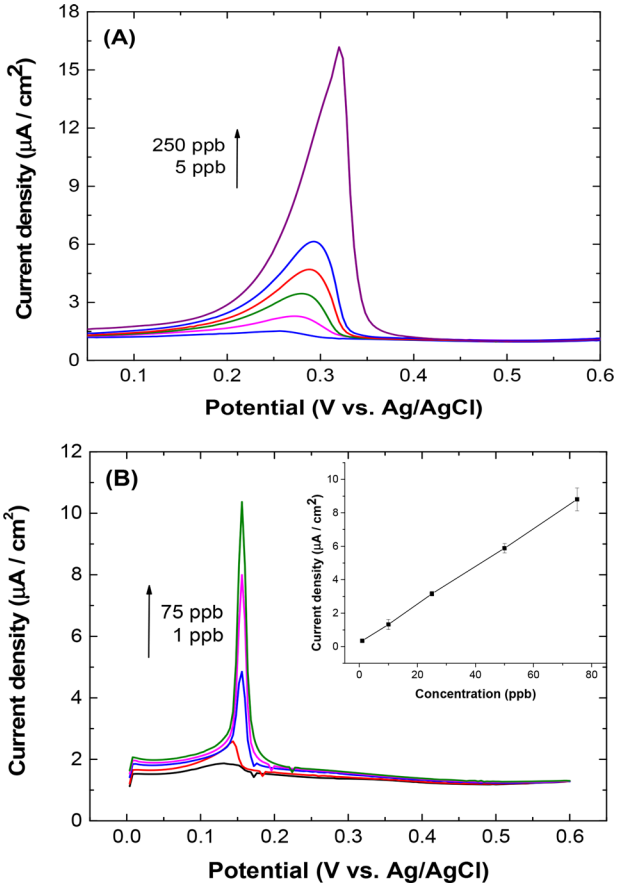

Figure 7. Differential pulse anodic stripping voltammetric (DPASV) i−E curves for standard solutions (1−250 μg L^{-1}) of Ag(I) in 0.1 mol L^{-1} acetate buffer (pH 4.6) at a (A) planar film and (B) BDD disk electrodes. The deposition potential was −0.3 V and the deposition time was 120 s. The curves were recorded using a pulse amplitude of 0.05 V; a potential step of 0.004 V; a pulse width of 50 ms; and a pulse period of 100 ms. Concentrations are shown as ppb (μg L^{-1}).

of the Ag(I) concentration for the (A) planar and (B) disk electrodes. Well-defined peaks are seen at 0.28 V for the planar electrode and 0.16 V for the disk electrode. The stripping peaks are considerably more narrow for the disk electrode with the oxidation current commencing around 0.15 V. The peak current increased, the peak width increased and the peak potential shifted positive with increasing solution concentration of Ag(I) for the planar film. This is attributed to increasing coverage of metal deposits during the deposition step and a widely varying deposit size across the surface.[2−4,49] The

DOI: 10.1021/acs.analchem.7b04983
Anal. Chem. 2018, 90, 6477−6485

rougher morphology and the distinct grain and grain boundary regions of the planar film electrode give rise to greater variability in the deposit size and the sites from which stripping occurs. Larger deposits take longer to dissolve than smaller ones once the oxidation potential has been reached, hence, the more positive peak potential with coverage.

In contrast, the stripping peak current increased with Ag(I) concentration for the disk electrode with a relatively unchanged peak potential and peak width. The disk electrode is more topographically homogeneous due to the polishing and this is believed to be the reason for the narrower and less positive stripping peak. Smaller nominal deposit sizes take less time to dissolve so the stripping peak potentials are less positive than the values for the planar film in the potential sweep measurements. The stripping peak currents increased linearly ($R^2 > 0.990$) for both electrodes proportionally with the Ag(I) solution concentration. The linear dynamic range for the disk electrode was from 1 to 75 $\mu g\ L^{-1}$ ($R^2 > 0.99$) and for the planar film electrode was from 5 to 250 $\mu g\ L^{-1}$ ($R^2 > 0.98$). Roll-off in the current response curve was observed for the disk electrode at solution concentrations greater than 75 $\mu g\ L^{-1}$. No roll-off was seen for the planar film electrode at the highest solution concentration measured, 250 $\mu g\ L^{-1}$. The inset in Figure 7B shows the response curve for the disk electrode.

Good linearity of the peak charge with concentration was also seen for both electrodes with a linear dynamic range ($R^2 > 0.98$) from 5 to 250 ppb Ag(I) for the planar film electrode and 1−75 ppb for the disk electrode. Roll-off in the linearity was seen for the disk electrode at solution concentrations above 75 ppb. The peak widths (full width at half-maximum, fwhm) range from 56 to 112 mV and from 16 to 68 mV for the planar and disk electrodes; greater width with increasing Ag(I) concentration.

Detection Figures of Merit. Table 1 presents a summary of the Ag(I) detection figures of merit for the two electrodes

Table 1. Detection Figures of Merit for Ag(I) Using a Planar Film and a Disk BDD Electrode

	disk BDD	planar BDD
background current (nA; 0.3 V)	35 ± 1	207 ± 1
noise (nA; 0.3 V)	4.7 ± 0.5	29 ± 1
LOD ($\mu g\ L^{-1}$), S/N = 3	0.7 ± 0.3	1.7 ± 0.8
sensitivity (nA L μg^{-1})	3.6 ± 0.7	10.6 ± 0.5
linear dynamic range ($\mu g\ L^{-1}$)	1−75	5−250
reproducibility (RSD %; 50 $\mu g\ L^{-1}$; $n = 3$)	4.7	3.4

obtained using standard solutions. The background current at the peak potential is lower by 6× for the disk electrode. This is due to a smaller real surface area. The noise at the detection potential is also 6× lower for the disk electrode. This is related to the difference in geometric areas of the two electrodes, which is ∼9× smaller for the disk electrode. The minimum concentrations detected experimentally were 1 and 5 $\mu g\ L^{-1}$, respectively, for the disk and film BDD electrodes. These values are close to the theoretical limits of detection (LOD) for each electrode at a signal-to-noise ratio (S/N) = 3. The calculated theoretical values were 1.7 and 0.7 $\mu g\ L^{-1}$ for the planar film and the disk electrode, respectively, for the deposition conditions used. The LOD was calculated according to the following equation:

$$\mathrm{LOD} = \frac{3(\sigma)}{m} \quad (1)$$

A summary of some literature data reported for Ag(I) detection by ASV is presented in Table 2. The LOD, which is just one of several important detection figures of merit, achieved with the disk electrode is comparable to that for a GaN electrode and lower than the values for some of the other electrodes. Once again, this demonstrates that the analysis of Ag(I) is suitable with BDD electrodes. Data for the colorimetric solid-phase extraction (C-SPE) method that has been tested on-board ISS are also presented. The method has a wider linear dynamic range but a comparable LOD as compared to the ASV method with the BDD disk electrode.

Table 2. Comparison of the Limit of Detection (LOD) for Ag(I) at Other Electrode Materials Using Anodic Stripping Voltammetry

	method	linear range ($\mu g\ L^{-1}$)	LOD ($\mu g\ L^{-1}$)
glassy carbon (hydrogen activated)[50]	ASV		5.4
GaN[47]	SWV	1−100	0.5
BDD planar film[2−4]	DPV	0.1−1000	0.1
graphite felt[51]	ASV	2.7−134	2.7
3C-SiC[52]	ASV	10−1000	4
edge plane pyrolytic graphite electrode[53]	DPASV	1−8	0.87
C-SPE[20]		5−1000	4

While we did not directly compare the performance of BDD with these other electrodes, the advantages of diamond for the detection of heavy metal ions by ASV are (i) the general lack of need for any surface pretreatment prior to use, (ii) the ability to use the electrode in complex media due to the material's fouling resistance, (iii) as good or superior detection figures of merit (linear dynamic range, limit of detection, response reproducibility and response stability over extended use), and (iv) weak interference from the reduction of dissolved oxygen.

Water Sample Analysis. The Ag(I) concentration in three water samples was determined: a NIST standard solution (SRM 1640), a NASA potable water sample, and a NASA iodinated water sample (no Ag(I) added). Detection was performed using both the disk and planar film BDD electrodes. The NASA potable water sample was diluted 5× and 25×, respectively, for the planar film and disk electrodes so that the expected concentration fell within the linear dynamic range established for both electrodes.

Figure 8 shows a DPASV $i-E$ curves for the three water samples, overlaid with curves for standard additions of Ag(I) at concentrations ranging from 5 to 100 $\mu g\ L^{-1}$ for the (A) planar film and (B) the disk electrode. The curves have not been background corrected. The stripping peaks for the NASA potable water and NIST samples are broad at the planar film electrode, in accordance with the peak shapes for the standard solutions presented above. The NASA iodinated water sample produced no peak, as expected because the solution contained no Ag(I). It was simply used as a control.

For the planar electrode, the NASA potable water sample presented a peak potential at 278 mV while the NIST reference solution presented a peak at 206 mV. The NASA potable water sample had a greater quantity of Ag(I) ions than the NIST sample, based qualitatively on the peak height and area. This

DOI: 10.1021/acs.analchem.7b04983
Anal. Chem. 2018, 90, 6477−6485

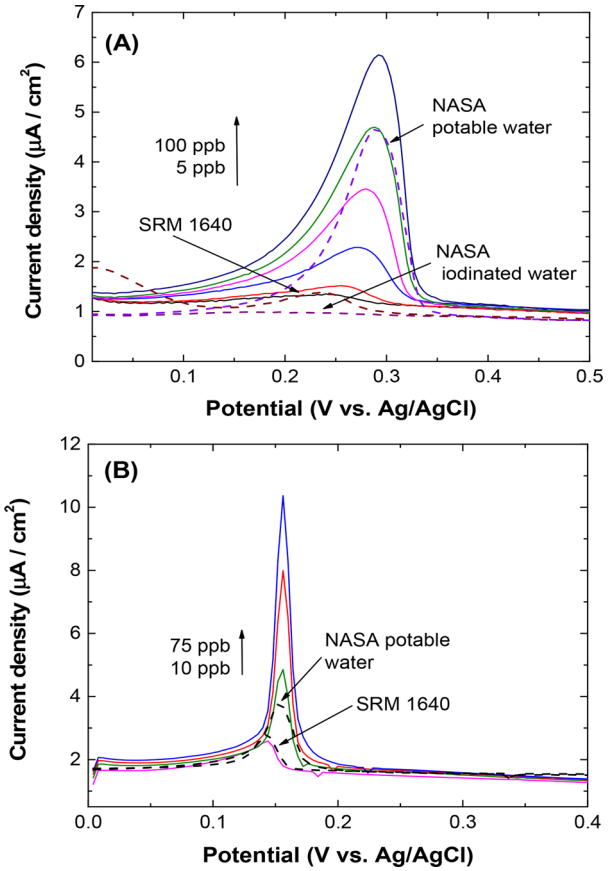

Figure 8. Differential pulse anodic stripping voltammetric (DPASV) *i*–*E* curves for a NASA potable water sample, a NIST standard solution (SRM 1640) and a NASA iodinated water sample overlaid with curves for standard additions of Ag(I) ranging in concentration from 5 to 100 μg L^{-1}. Panel (A) shows the curves recorded with the BDD film electrode and panel (B) shows curves recorded with the BDD disk electrode. The supporting electrolyte was 0.1 mol L^{-1} acetate buffer (pH 4.6). The deposition potential was −0.3 V and the deposition time was 120 s. The curves were recorded by differential pulse voltammetry using a pulse amplitude of 0.05 V; a potential step of 0.004 V; a pulse width of 50 ms; and a pulse period of 100 ms. Concentrations are shown as ppb (μg L^{-1}).

higher metal phase coverage leads to a more positive stripping potential. The stripping peaks obtained with the disk electrode were sharper than the peaks for the planar film electrode, as was the case with the standard solutions. In all cases, the peak current and charge increased proportionally (R^2 > 0.99) with the solution concentration.

Table 3 presents DPASV-determined concentrations for the NASA potable and NIST standard water samples. The concentrations were determined from response curves generated by the standard addition method. Three samples of each analyte were measured and the concentrations determined. The concentrations determined by DPASV were compared with those determined by ICP-OES using an external standard method. The analysis of Ag(I) in the NASA potable water yielded statistically similar values of 424 ± 22 and 431 ± 17 μg L^{-1} for the disk and the planar film electrodes, respectively. The percent error in the responses, as compared to the true value as specified by NASA (422 μg L^{-1}), is small for both electrodes, 0.5% and 2.1%, respectively, for the planar film and disk electrodes. ICP-OES analysis yielded a concentration of 425 ± 5 μg L^{-1}. For this sample, the electrochemical and ICP methods produced virtually values for the concentration.

Table 3. Concentration (μg L^{-1}) of Ag(I) in Real Water Samples[a]

	NASA potable water	NIST 1640
ICP	425 ± 5	8.1 ± 0.7
disk	424 ± 22	6.1 ± 0.1
planar	431 ± 17	6.2 ± 0.4

[a]Values presented are mean ± uncertainty for *n* = 3 measurements of each sample.

The NIST SRM 1640 standard was a complex sample with more than 24 ionic species and metal ions present.[3] The certificated Ag(I) concentration at the time of preparation was 7.62 ± 0.25 μg L^{-1}.[3] The DPASV analysis of Ag(I) in this solution yielded concentrations of 6.1 ± 0.1 and 6.2 ± 0.4 μg L^{-1}, respectively, for the disk and the planar BDD electrodes. Previously, when this sample was measured by DPASV using diamond film electrodes, a concentration of 8.04 ± 0.73 μg L^{-1} was determined.[3] Both current values are statistically similar but are slight underestimates of the true value. The error in concentration for both electrodes is ∼19%. In contrast, the Ag(I) concentration determined by ICP-OES produced a concentration of 8.1 ± 0.7 μg L^{-1}, which is slightly higher than the expected value. The error in this measurement is only 6%. It is supposed the underestimate of the solution concentration by DPASV is due to some colloidal Ag formation that occurred over time. The electrochemical method is insensitive to colloidal Ag. The overestimate of the concentration by ICP is likely due to some water evaporation over the sample life, which would produce an increased solution concentration of total Ag. The ICP method is sensitive to both colloidal Ag and Ag(I) dissolved in solution.

CONCLUSIONS

The following are the key findings from the work, which validate the performance of the new BDD disk electrode: (1) The boron-doped diamond disk electrode was found to be useful for trace Ag(I) analysis by DPASV. The smooth surface morphology produced by the mechanical polishing (nm roughness) is advantageous for achieving narrow stripping peaks. (2) The disk electrode was durable with repeated use as the seal between the diamond and PEEK holder remained intact. (3) The optimum detection conditions were a −0.3 V deposition potential, a 120 s deposition time, and a scan rate of 40 mV/s. (4) The detection figures of merit for the disk electrode were as good or superior to those of a boron-doped diamond planar thin-film electrode. Detection limits were ≤5 μg L^{-1} (S/N = 3) for the modest deposition conditions, and response variabilities were <5% RSD. On the other hand, the disk electrode presented a more limited linear dynamic range because of the reduced surface area available for metal phase formation. (5) The detection limit for Ag(I) at the disk electrode (∼1 μg L^{-1}, S/N = 3) was not quite as low as the value previously reported for planar diamond film electrodes, albeit using a different set of deposition conditions.[2,3] (6) The BDD disk electrode and the ASV method meet both the E.P.A. sMCL of 100 μg L^{-1} for Ag(I) and the effective NASA concentration range of 300−500 μg L^{-1}. (7) DPASV with the disk electrode produced accurate values for the Ag(I) concentration in a NASA potable water sample, in agreement

DOI: 10.1021/acs.analchem.7b04983
Anal. Chem. 2018, 90, 6477−6485

with ICP-OES results. DPASV with the disk electrode slightly underestimated the concentration in a NIST standard presumably due to some colloidal Ag formation.

■ ASSOCIATED CONTENT

Supporting Information

The Supporting Information is available free of charge on the ACS Publications website at DOI: 10.1021/acs.analchem.7b04983.

Electrochemical characterization data for $Fe(CN)_6^{3-/4-}$, Raman spectra, and SEM images of the metal-coated diamond film electrode (PDF).

■ AUTHOR INFORMATION

Corresponding Author

*E-mail: swain@chemistry.msu.edu. Phone: +1-517-353-1090. Fax: 517-353-1793.

ORCID

Cory A. Rusinek: 0000-0002-6852-0219

Greg M. Swain: 0000-0001-6498-8351

Author Contributions

All authors have given approval to the final version of the manuscript.

Notes

The authors declare no competing financial interest.

■ ACKNOWLEDGMENTS

The research was carried out under the framework of Project No. W911-NF-14-10063 funded by the Army Research Office (G.M.S.). The support from the Escuela Politécnica Nacional is hereby acknowledged for providing a research fellowship (V.Y.M.). We thank Dr. Kathryn Severin and Brandon Whitman (Department of Chemistry, MSU) for their help with the use of ICP-OES and SEM, respectively. We also thank Michael Becker (Fraunhofer Center for Coatings and Diamond Technologies) for his guidance in preparing the disk electrode.

■ REFERENCES

(1) Bansod, B.; Kumar, T.; Thakur, R.; Rana, S.; Singh, I. *Biosens. Bioelectron.* **2017**, *94*, 443−455.

(2) Show, Y.; Witek, M. A.; Sonthalia, P.; Swain, G. M. *Chem. Mater.* **2003**, *15*, 879−888.

(3) Sonthalia, P.; McGaw, E.; Show, Y.; Swain, G. M. *Anal. Chim. Acta* **2004**, *522*, 35−44.

(4) Mcgaw, E. A.; Swain, G. M. *Anal. Chim. Acta* **2006**, *575*, 180−189.

(5) Song, Y.; Swain, G. M. *Anal. Chim. Acta* **2007**, *593*, 7−12.

(6) Song, Y.; Swain, G. M. *Anal. Chem.* **2007**, *79*, 2412−2420.

(7) El-Mai, H.; Espada-Bellido, E.; Stitou, M.; García-Vargas, M.; Galindo-Riaño, M. D. *Talanta* **2016**, *151*, 14−22.

(8) Setyawati, M. I.; Yuan, X.; Xie, J.; Leong, D. T. *Biomaterials* **2014**, *35*, 6707−6715.

(9) Zhou, Y.-G.; Rees, N. V.; Compton, R. G. *Angew. Chem., Int. Ed.* **2011**, *50*, 4219−4221.

(10) Zhang, T.; Chai, Y.; Yuan, R.; Guo, J. *Mater. Sci. Eng., C* **2012**, *32*, 1179−1183.

(11) Beer, C.; Foldbjerg, R.; Hayashi, Y.; Sutherland, D. S.; Autrup, H. *Toxicol. Lett.* **2012**, *208*, 286−292.

(12) Gumpu, M. B.; Sethuraman, S.; Krishnan, U. M.; Rayappan, J. B. B. *Sens. Actuators, B* **2015**, *213*, 515−533.

(13) Silvestry-Rodríguez, N.; Sicairos-Ruelas, E. E.; Gerba, C. P.; Bright, K. R. *Rev. Environ. Contam. Toxicol.* **2007**, *191*, 23−45.

(14) Boudreau, M. D.; Imam, M. S.; Paredes, A. M.; Bryant, M. S.; Cunningham, C. K.; Felton, R. P.; Jones, M. Y.; Davis, K. J. *Toxicol. Sci.* **2016**, *150*, 131−160.

(15) E.P.A. website, Secondary Drinking Water Standards, www.epa.gov.

(16) Hill, A. A.; Lipert, R. J.; Porter, M. D. *Talanta* **2010**, *80*, 1606−1610.

(17) Plumlee, D. K.; Mudgett, P. D.; Schultz, J. R. 33rd International Conference on Environmental Systems, Vancouver, B.C., Canada, (2003). (SAE Technical Paper #2003−01−2401).

(18) Gazda, D. B.; Schultz, J. R.; Siperko, L. M.; Porter, M. D.; Flint, S. M.; McCoy, J. T. In-Flight Water Quality Monitoring on the International Space Station (ISS): Measuring Biocide Concentrations with Colorimetric Solid-Phase Extraction. *41st International Conference on Environmental Systems, 2011*; ICES, 2011.

(19) Gazda, D. B.; Nolan, D. J.; Rutz, J. A.; Schultz, J. R.; Siperko, L. M.; Porter, M. D.; Lipert, R. J.; Flint, S. M.; McCoy, J. T. Design, Certification and Development of the Colorimetric Water Quality Monitoring Kit (CWQMK). *AIAA Technical Paper #AIAA-2010−6044*, 2010.

(20) Arena, M. P.; Porter, M. D.; Fritz, J. S. *Anal. Chim. Acta* **2003**, *482*, 197−207.

(21) Gazda, D. B.; Fritz, J. S.; Porter, M. D. *Anal. Chem.* **2004**, *76*, 4881−4887.

(22) Hill, A. A.; Lipert, R. J.; Porter, M. D. *Talanta* **2010**, *80*, 1606−1610.

(23) Demars, R. D.; Shain, I. *Anal. Chem.* **1957**, *29*, 1825−1827.

(24) Florence, T. M. *J. Electroanal. Chem. Interfacial Electrochem.* **1970**, *27*, 273−281.

(25) Zeng, B.; Ding, X.; Pan, D.; Zhao, F. *Talanta* **2003**, *59*, 501−507.

(26) Wang, J.; Lu, J.; Hocevar, S. B.; Farias, P. A. M.; Ogorevc, B. *Anal. Chem.* **2000**, *72*, 3218−3222.

(27) Zhao, D.; Wang, T.; Han, D.; Rusinek, C.; Steckl, A. J.; Heineman, W. R. *Anal. Chem.* **2015**, *87*, 9315−9321.

(28) Janegitz, B. C.; Marcolino-Junior, L. H.; Campana-Filho, S. P.; Faria, R. C.; Fatibello-Filho, O. *Sens. Actuators, B* **2009**, *142*, 260−266.

(29) Bassie, T.; Siraj, K.; Tesema, T. E. *Adv. Sci., Eng. Med.* **2013**, *5*, 275−284.

(30) Hao, C.; Shen, Y.; Shen, J.; Xu, K.; Wang, X.; Zhao, Y.; Ge, C. *Microchim. Acta* **2016**, *183*, 1823−1830.

(31) Dong, S.; Wang, Y. *Anal. Chim. Acta* **1988**, *212*, 341−347.

(32) Mohadesi, A.; Taher, M. A. *Talanta* **2007**, *71*, 615−619.

(33) O'Neil, G. D.; Newton, M. E.; Macpherson, J. V. *Anal. Chem.* **2015**, *87*, 4933−4940.

(34) Arantes, T. M.; Sardinha, A.; Baldan, M. R.; Cristorvan, F. H.; Ferreira, N. G. *Talanta* **2014**, *128*, 132−140.

(35) Hutton, L. A.; Newton, M. E.; Unwin, P. R.; Macpherson, J. V. *Anal. Chem.* **2011**, *83*, 735−745.

(36) El Tall, O.; Jaffrezie-Renault, N.; Sigaud, M.; Vitorri, O. *Electroanalysis* **2007**, *19*, 1152−1159.

(37) Manivannan, A.; Kawasaki, R.; Tryk, D. A.; Fujishima, A. *Electrochim. Acta* **2004**, *49*, 3313−3318.

(38) Zeng, A.; Liu, E.; Tan, S. N.; Zhang, S.; Gao, J. *Electroanalysis* **2002**, *14*, 1294−1298.

(39) Prado, C.; Wilkins, S. J.; Marken, F.; Compton, R. G. *Electroanalysis* **2002**, *14*, 262−272.

(40) Macpherson, J. V. *Phys. Chem. Chem. Phys.* **2015**, *17*, 2935−2949.

(41) Einaga, Y.; Foord, J. S.; Swain, G. M. *MRS Bull.* **2014**, *39*, 525−532.

(42) Wang, S.; Butler, J. E.; Swain, G. M. *Diamond Relat. Mater.* **2009**, *18*, 669−677.

(43) Granger, M. C.; Xu, J.; Strojek, J. W.; Swain, G. M. *Anal. Chim. Acta* **1999**, *397*, 145−161.

(44) Xu, J.; Granger, M. C.; Chen, Q.; Strojek, J. W.; Lister, T. E.; Swain, G. M. *Anal. Chem.* **1997**, *69*, 591A−597A.

(45) Xu, J.; Chen, Q.; Swain, G. M. *Anal. Chem.* **1998**, *70*, 3146−3154.

DOI: 10.1021/acs.analchem.7b04983
Anal. Chem. 2018, 90, 6477−6485

(46) Chen, Q.; Swain, G. M. *Langmuir* **1998**, *14*, 7017−7026.
(47) Zhang, M.-R.; Pan, G.-B. *Talanta* **2017**, *165*, 540−544.
(48) Pletcher, D. *A First Course in Electrode Processes*; The Royal Society of Chemistry, 2009.
(49) Bennett, J. A.; Show, Y.; Wang, S. H.; Swain, G. M. *J. Electrochem. Soc.* **2005**, *152*, E184−E192.
(50) Přibil, R.; Štulíková, M. *Talanta* **1987**, *34*, 705−708.
(51) Davies, T. J. *Analyst* **2016**, *141*, 4742−4748.
(52) Zhuang, H.; Wang, C.; Huang, N.; Jiang, X. *Electrochem. Commun.* **2014**, *41*, 5−7.
(53) Wantz, F.; Banks, C. E.; Compton, R. G. *Electroanalysis* **2005**, *17*, 655−661.

DOI: 10.1021/acs.analchem.7b04983
Anal. Chem. 2018, 90, 6477−6485